JOURNAL OF GEOPHYSICAL RESEARCH, VOL. 114, D24110, doi:10.1029/2009JD011803, 2009

Intermodel variability of future changes in the Baiu rainband estimated by the pseudo global warming downscaling method

Hiroaki Kawase,[1] Takao Yoshikane,[2] Masayuki Hara,[2] Fujio Kimura,[2,3] Tetsuzo Yasunari,[2,4] Borjiginte Ailikun,[5] Hiroaki Ueda,[6] and Tomoshige Inoue[6]

Received 26 January 2009; revised 10 August 2009; accepted 27 August 2009; published 31 December 2009.

[1] Changes in the Baiu rainband owing to global warming are assessed by the pseudo global warming downscaling method (PGW-DS). The PGW-DS is similar to the conventional dynamical downscaling method using a regional climate model (RCM), but the boundary conditions of the RCM are obtained by adding the difference between the future and present climates simulated by coupled general circulation models (CGCMs) into the 6-hourly reanalysis data in a control period. We conducted the multiple PGW-DS runs using the selected Coupled Model Intercomparison Project Phase 3 (CMIP3) multimodel data set, giving better performance around East Asia in June, and the PGW-DS run using the multiselected CGCM model ensemble mean (PGW-MME run). The PGW-MME and PGW-DS runs show an increase in precipitation over the Baiu rainband and the southward shift of the Baiu rainband. The PGW-MME run has good similarity to the average of all PGW-DS runs. This fact indicates that an average of the multiple PGW-DS runs can be replaced by a single PGW-DS run using the multiselected CGCM ensemble mean, reducing the significant computational expense. In comparison with the GCM projections, the PGW-DS runs reduce the intermodel variability in the Baiu rainband caused by the CGCMs themselves.

Citation: Kawase, H., T. Yoshikane, M. Hara, F. Kimura, T. Yasunari, B. Ailikun, H. Ueda, and T. Inoue (2009), Intermodel variability of future changes in the Baiu rainband estimated by the pseudo global warming downscaling method, *J. Geophys. Res.*, *114*, D24110, doi:10.1029/2009JD011803.

1. Introduction

[2] The Baiu/Meiyu/Changma front, as it called in Japan/China/Korea, is strongly related to the Asian Summer Monsoon (ASM) and brings a large amount of rainfall over East Asia in summer (hereafter, referred to as the Baiu rainband) [*Kurashima and Hiranuma*, 1971]. The climatic variation in the Baiu rainband causes not only frequent serious flooding but also occasional droughts in East Asia. The *Intergovernmental Panel on Climate Change* (*IPCC*) [2001, 2007] reported that the increase in greenhouse gases could change the ASM intensity and duration, resulting in changes in the Baiu rainband in the future.

[3] The Ocean-Atmosphere Coupled General Circulation Models (CGCMs) have been used to investigate climate changes owing to an increase of greenhouse gases. The analysis method using the multiple CGCM model ensemble mean (hereafter, the MME mean) is effective for the improvement of projections owing to the reduction of biases and uncertainties of individual CGCMs [e.g., *Giorgi and Mearns*, 2002]. Climate changes were investigated using the MME mean obtained from the WCRP Coupled Model Intercomparison Project Phase 3 (CMIP3) multimodel data set [*Meehl et al.*, 2007] during the ASM season [*Min et al.*, 2004; *Ueda et al.*, 2006; *Kitoh and Uchiyama*, 2006]. The activity of the ASM would be enhanced in association with the strengthening of anticyclonic circulations to its south and north [*Kimoto*, 2005], resulting in the change in the Baiu rainband.

[4] The simulation of the Baiu rainband is extremely difficult for GCMs owing to the lack of resolution as well as to shortcomings in the physical process parameterizations [*Kang et al.*, 2002; *Ninomiya et al.*, 2002]. *Kawatani and Takahashi* [2003] demonstrated that the structures of the Baiu front, from large scale to mesoalpha scale, were well simulated in a high-resolution AGCM with a grid size of about 110 km. A comparison of high- and medium-resolution CGCMs showed that the higher-resolution version better reproduced not only the mean precipitation but also the frequency of precipitation over Japan in the warm season in the present climate [*Kimoto et al.*, 2005]. The time-slice experiment was conducted using a very high-resolution AGCM with 20 km grid size developed by the Japan

[1]Atmospheric Physics Section, Atmospheric Environment Division, National Institute for Environmental Studies, Tsukuba, Japan.
[2]Research Institute for Global Change, Japan Agency for Marine-Earth Science and Technology, Yokohama, Japan.
[3]Also at Graduate School of Life and Environmental Sciences, University of Tsukuba, Tsukuba, Japan.
[4]Also at Hydrospheric Atmospheric Research Center, Nagoya University, Nagoya, Japan.
[5]Institute of Atmospheric Physics, Chinese Academy of Science, Beijing, China.
[6]Graduate School of Life and Environmental Sciences, University of Tsukuba, Tsukuba, Japan.

0148-0227/09/2009JD011803$09.00

Meteorological Agency (JMA) and the Meteorological Research Institute (MRI) (hereafter, MRI 20 km AGCM) [*Mizuta et al.*, 2006]. In comparison with lower-resolution model experiments, the MRI 20 km AGCM showed superiority in simulating orographic rainfall regarding not only its location but also its amount [*Kusunoki et al.*, 2006].

[5] Downscaling methods are the techniques to complement the GCM simulations with the detailed temporal and spatial structures. Two major downscalings have been proposed: one is a statistical downscaling, and the other is a dynamical downscaling (DDS). A conventional DDS consists of a numerical simulation using a regional climate model (RCM). The RCM applies the GCM outputs to the initial and boundary conditions. *Wang et al.* [2004] stated the history of the development of DDSs. Original RCMs were conducted using the hydrostatic primitive equations. With the development of computational performances, some RCMs have been converted into models on the basis of nonhydrostatic equations. *Kato et al.* [2001] were concerned that the regional climate changes were mainly influenced by the reproducibility of the present climate simulated by the GCM and indicated that the GCM should be of a good quality when the regional climate was estimated in detail by the DDSs.

[6] Using the RCM with a 20 km grid size, *Kurihara et al.* [2005] indicated that the precipitation would increase during the warm season in Western Japan because the intensification of the anticyclonic circulation over the east Pacific Ocean resulted in strong moisture flux convergence over Western Japan in the late 21st Century under the Special Report on Emissions Scenario A2 (SRES-A2) scenario by *IPCC* [2000]. More detailed changes in the Baiu rainband owing to global warming were investigated using a nonhydrostatic cloud-resolving regional climate model (NHM). The initial and lateral boundary conditions were obtained from the outputs of the MRI 20 km AGCM under the SRES-A1B scenario [*Yasunaga et al.*, 2006]. The Baiu front was likely to stay over the southern Japan Islands and did not move northward in summer in the global warming climate [*Yoshizaki et al.*, 2005].

[7] A new concept of the DDS called pseudo global warming downscaling method (hereafter PGW-DS) was proposed by *Kimura and Kitoh* [2007] and adopted for some regions [*Sato et al.*, 2007; *Hara et al.*, 2008]. The PGW-DS is almost the same as the conventional DDS, but the boundary condition of the RCM is a composite of 6-hourly reanalysis data and the differences in monthly mean variables between the present and the future climates simulated by CGCMs. *Knutson et al.* [2008] applied a similar method to the Atlantic hurricanes and found that Atlantic hurricane and tropical storm frequencies would be reduced and near-storm rainfall rates would increase substantially under the pseudo atmospheric state and sea surface temperature (SST) in the 21st century. *Frei et al.* [1998] conducted a similar DDS to the PGW-DS to investigate heavy precipitation processes in a warmer climate in Europe, but they considered only the effects of uniform temperature rise and relevant changes in other atmospheric variables.

[8] *Kawase et al.* [2008] applied the PGW-DS to the past climatic change in the distribution of the Baiu rainband over China between the 1960s and 1990s during early summer. They discussed two advantages of the PGW-DS. One is the reduction of the model bias contained in the GCMs, and the other is the circumventing of the uncertainty caused by the interannual variability even in the case of a shorter integration period, such as 10 years. It is, however, difficult to evaluate the changes in the interannual variability and the frequencies of disturbances because the PGW-DS assumes unchanged variability even in the future climate. The uncertainty caused by the change in the variability still remains.

[9] The PGW-DS easily enables multiple DDSs under multiple CGCMs because it requires only monthly mean atmospheric variables and sea surface temperature, both of which can be much more easily obtained than 6-hourly data. This reduces the need to archive and access CGCM data. The purpose of this study is to assess future changes in the Baiu rainband using the PGW-DS. We focus on June when the stable Baiu rainband appears around Southern China and Japan.

2. Reproducibility of Present Climate and Projections by CGCMs

[10] The CGCMs have various biases in the simulation of present regional climate, e.g., in East Asia, which would result in a large uncertainty in the projections of regional climate change owing to global warming. The PGW-DS relies on the differences between present and future climates simulated by CGCMs. The selection of CGCMs with high performance of the present climate is essential to conduct the PGW-DS, although this method reduces the effects of the CGCM bias in the present climate more than the conventional DDS.

[11] A new type of diagram (hereafter, the Taylor diagram) and skill scores were proposed by *Taylor* [2001] to evaluate CGCM performances. The Taylor diagram relates the centered Root Mean Square Error (RMSE), the pattern correlation, and the standard deviation. The performances of CGCMs in Asia have also been evaluated using the Taylor diagram in previous studies [*Min et al.*, 2004; *Kusunoki et al.*, 2006; *Inoue and Ueda*, 2009]. The Taylor diagram and skill score make it possible to evaluate the location and strength of the Baiu rainband simulated by the CGCMs.

[12] Table 1 shows the 15 CGCMs with the necessary atmospheric and surface variables to conduct the PGW-DS, which are available at the CMIP3 multimodel data set. The present climate is obtained from the 20th Century Climate in Coupled Models (20C3M). References of precipitation and 850 hPa wind are derived from CPC Merged Analysis of Precipitation (CMAP) [*Xie and Arkin*, 1997] and ECMWF 40-year Re-Analysis (ERA40) Data [*Uppala et al.*, 2005], respectively. We define the analyzed period as 1980–1999 for comparison with CMAP precipitation data. The analyzed area is region A, shown in Figure 1. All models are interpolated into the same $2.5^\circ \times 2.5^\circ$ grids as the reference data.The skill score (S) is defined as

$$S = \frac{4(1+R)^4}{(SDR + 1/SDR)^2 (1+R_0)^4},$$

Table 1. Fifteen CMIP3 Multimodel Data Sets Having Enough Atmospheric Variables to Conduct the PGW-DS

Model	CMIP3 I.D.	Originating Group(s)	Country
CCCMA	CGCM3.1(T47)	Canadian Centre for Climate Modeling and Analysis	Canada
CCSM	CCSM3	National Center for Atmospheric Research	United States
CNRM	CNRM-CM3	Meteo-France, Centre National deRecherches Météorologiques	France
GFDL20	GFDL-CM2.0	U.S. Department of Commerce, NOAAGeophysical Fluid Dynamics Laboratory	United States
GFDL21	GFDL-CM2.1		
GISS-EH	GISS-EH	NASA Goddard Institute for Space Studies	United States
GISS-ER	GISS-ER		
IAP	FGOALS-g1.0	LASG/Institute of Atmospheric Physics	China
INGV	INGV-SXG	Instituto Nazionale di Geofisica e Vulcanologia	Italy
INM	INM-CM3.0	Institute for Numerical Mathematics	Russia
IPSL	IPSL-CM4	Institut Pierre Simon Laplace	France
MIROCH	MIROC3.2(hires)	Center for Climate System Research,	Japan
MIROCM	MIROC3.2(medres)	University of Tokyo,	
		National Institute for Environmental Studies,	
		and Frontier Research Center for Global Change (JAMSTEC)	
MRI	MRI-CGCM2.3.2	Meteorological Research Institute	Japan
PCM	PCM	National Center for Atmospheric Research	United States

where R, R_0, and SDR are the correlation coefficient, the maximum correlation attainable, which is equal to the mean of the intraensemble correlation values, and the model standard deviation divided by the standard deviation of the corresponding observed field [*Taylor*, 2001], respectively. Here, we assume $R_0 = 1.0$. High skill scores mean that the spatial patterns of the realistic climate are well simulated by the CGCMs. More detailed information is provided in the work of *Taylor* [2001]. We select seven CGCMs, i.e., CCCMA, CNRM, GFDL21, INGV, MIROCM, MIROCH, and MRI, which have higher skill scores for precipitation than the average of all models. Both the MIROCM and the MIROCH are selected to focus on the difference in resolutions, but we only use one later version of the GFDL model, GFDL21.

[13] The seven selected CGCMs show higher correlation coefficients for precipitation in the range between 0.6 and 0.8 than the other CGCMs (Figure 2a). However, the standard deviations of the selected CGCMs are smaller than those of the reference data, except for the MIROCH and the MRI. The skill score of the ensemble mean of the seven CGCMs (hereafter, MME-CGCM) is the highest in Figure 2a, as reported in previous studies [e.g., *Min et al.*, 2004].

[14] The selected CGCMs, except for CCCMA, show quite high correlation coefficients of about 0.9 for the 850 hPa zonal wind component (Figure 2b). Their standard deviations are, however, scattered. The standard deviations of the MRI and the GFDL are similar to those of the reference data. The selected CGCMs are plotted more scattered on the Taylor diagram for the meridional wind component (Figure 2c) than for the zonal wind component. The MME-CGCM shows the highest skill score for the zonal and meridional winds as well as the precipitation.

[15] Figure 3 shows 30-year mean precipitation in June from 2060 to 2089 simulated by the MME-CGCM and the seven selected CGCMs under the SRES-A1B scenario. The rainband corresponding to the Baiu rainband is located from southern China to Japan in the MME-CGCM (Figure 3a). The MIROCM is similar to the MIROCH, but the amount of precipitation in the MIRCOM is much weaker than that in the MIROCH (Figures 3g and 3h), which depends on their resolutions [*Kawatani and Takahashi*, 2003]. Most CGCMs do not simulate the Baiu rainbands clearly (Figures 3b–3g), but only the MIROCH does (Figure 3h). Some CGCMs could not accurately simulate the Baiu rainband in the present climate (figure not shown), resulting in the obscure Baiu rainband in the future climate. Considering that we selected the CGCMs with higher performance in East Asia from the CMIP3 multimodel data set, the other CGCMs simulate the Baiu rainbands more poorly.

[16] Figure 4 shows the differences in the 30-year mean June precipitation between the 20C3M for the present climate (1970–1999) and the SRES-A1B scenario for the future climate (2060–2089). The MME-CGCM indicates an increase in precipitation over middle- and high-latitude regions, especially near the Baiu rainband, and a decrease in precipitation over the low-latitude region (Figure 4a). The change in precipitation of the MME-CGCM is, however, quite different from the changes in the individual CGCMs. The GFDL and the MRI show a decrease in precipitation (Figures 4c and 4e), while the CCCMA, MIROCM, and MIROCH show an increase in precipitation over Japan. Only the INGV shows a decrease in precipitation over Northern China (Figure 4d). The MIROCH and the

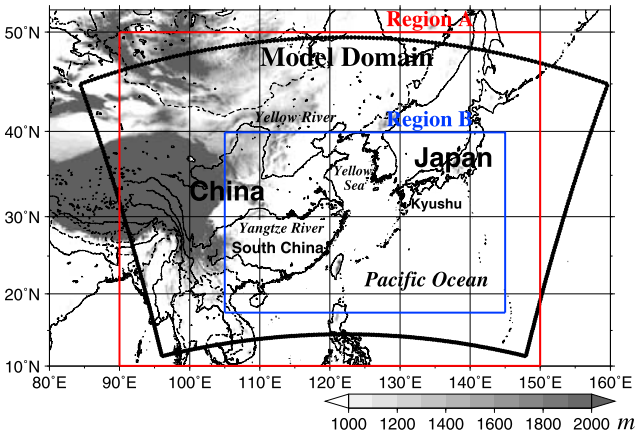

Figure 1. Geographical map of the analysis area. Areas enclosed by black, red, and blue lines represent the model domain, region A, and region B, respectively.

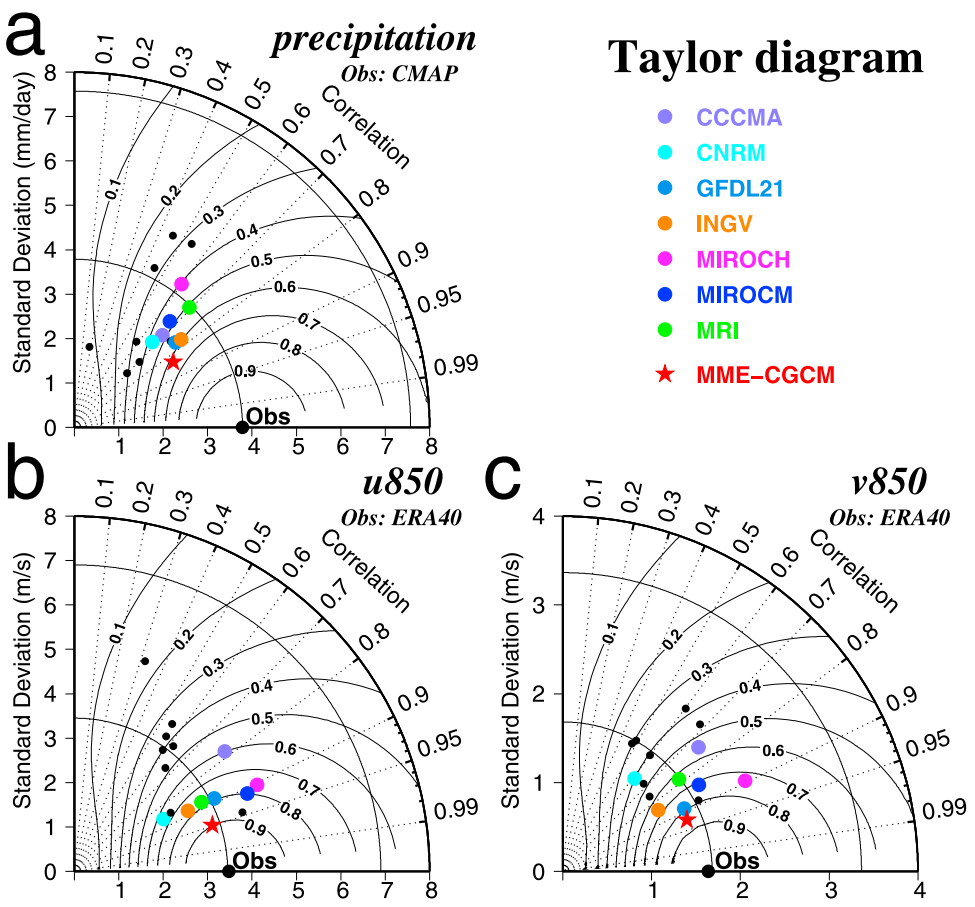

Figure 2. Taylor diagrams for the June climatological precipitation and 850 hPa wind (1980–1999) for East Asia. Large colored circles represent the seven selected models, and small black circles represent the other models.

MIROCM project similar changes in precipitation except for the amount (Figures 4g and 4h).

3. Procedure of a Pseudo Global Warming Downscaling Method

[17] A control run was conducted to simulate the Baiu rainband in the control period, which is the 1990s in this paper. We used the Advanced Research of Weather Research and Forecasting (WRF) model version 2.2 [*Skamarock et al.*, 2005]. The ERA40 data was applied to the initial and boundary conditions of the WRF model (CTRL-ERA40 run). The specifications of the numerical simulations are summarized in Table 2. The model domain was covered by 300 × 200 grids with 20 km grid intervals (Figure 1). The simulation was executed from 22 May to 1 July for each year. The first 10-day period was defined as a spin-up duration. Physical processes of the surface layer, boundary layer, and land surface were calculated by the Monin-Obukhov (Janjic Eta) scheme (Z. I. Janjic, The surface layer in the NCEP Eta model, Preprint, 11th Conference on Numerical Weather Prediction, pp. 354–356, Am. Meteorol. Soc., Norfolk, Va., 1996), the Mellor-Yamada-Janjic (Eta) TKE scheme [*Janjic*, 2002], and the Noah land surface scheme [*Chen and Dudhia*, 2001], respectively. Both the Kain-Fritsch convective parameterization scheme [*Kain and Fritsch*, 1993] and the WRF single-moment microphysics scheme (WSM6) [*Hong and Lim*, 2006] were activated as the precipitation process.

[18] Next, the present climatic fields, including the wind, temperature, geopotential height, surface pressure, and sea surface temperature, were calculated by the 30-year monthly mean from 1970 to 1999 in the 20C3M, as in section 2. Here, we used one ensemble member in each CGCM. The future climatic fields were calculated by the 30-year monthly mean from 2060 to 2089 under the SRES-A1B scenario. The pseudo future 6-hourly data set was obtained by adding the components of the climatic change between the present and future climates into the 6-hourly ERA40 data in the 1990s. The climate of the pseudo future data set corresponds to the future climate (2060–2089), while the variability, such as short-term disturbances and interannual variability, is similar to that in the 1990s. The PGW-DS runs were conducted using the pseudo future 6-hourly data. The flowchart of the PGW-DS is summarized in Figure 5.

[19] The relative humidity of the future climate was assumed to be equal to that of the present climate, which means that the absolute amount of water vapor was expected to increase owing to global warming because the saturation vapor pressure increases with temperature (i.e., the Clausius-Clapeyron relation). It has often been suggested that the distribution of relative humidity should remain roughly constant in the warming climate because the global trend of near-surface relative humidity is very

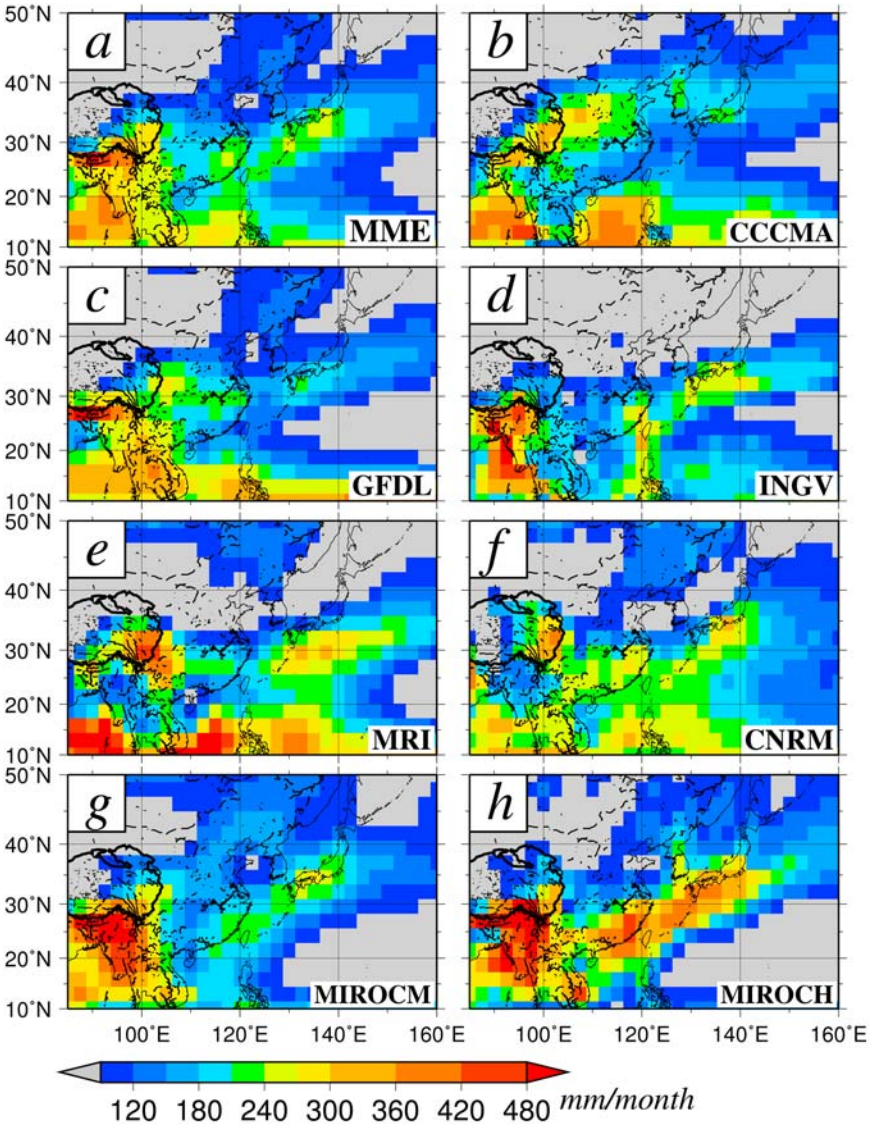

Figure 3. Thirty-year mean precipitation in June from 2060 to 2089 simulated by seven CGCMs and MME-CGCM under the SRES A1B scenario.

small during recent decades [*Dai*, 2006; *Trenberth*, 2005] and there is no detectable trend in relative humidity in the upper troposphere [*Soden et al.*, 2005].

[20] We conducted seven PGW-DS runs using the seven CGCMs selected in section 2, i.e., the PGW-CCCMA, PGW-CNRM, PGW-INGV, PGW-GFDL, PGW-MIROCM, PGW-MIROCH, and PGW-MRI runs. In addition, another PGW-DS run, called the PGW-MME run, was conducted using the MME-CGCM. We estimated future climatic changes in the Baiu rainband with a comparison of the CTRL-ERA40 run with the seven PGW-DS runs and the PGW-MME run.

[21] Considering the linear approximation, the pseudo future 6-hourly data satisfies the hydrostatic equilibrium, the equation of continuity, and the linear terms of dynamical equations. However, the balance of nonlinear terms, such as an advection term, is slightly disrupted. The PGW-DS applies the pseudo future 6-hourly data to only the initial and lateral boundary conditions. The imbalanced error caused by the nonlinear term seems to be smaller than the imbalanced errors between the lateral boundary conditions and interior mesh values.

[22] A simple numerical experiment was also conducted to investigate the impact of only the temperature rise on the Baiu rainband (TEMP-RISE run), as in the work of *Frei et al.* [1998]. The initial and boundary conditions were provided by the 6-hourly ERA40 data in the 1990s, but 3K in atmospheric temperature at all vertical levels and 2.2K at the sea surface temperature were added; these were comparable to the temperature rise at lower atmospheric levels and the sea surface in the MME-CGCM at the end of 21st Century under the SRES-A1B scenario. The geopotential height was recalculated according to the temperature rise.

4. Results of Downscalings

4.1. Observations and Control Run

[23] Figure 6a shows the distributions of the 10-year mean precipitation in June during the 1990s observed by

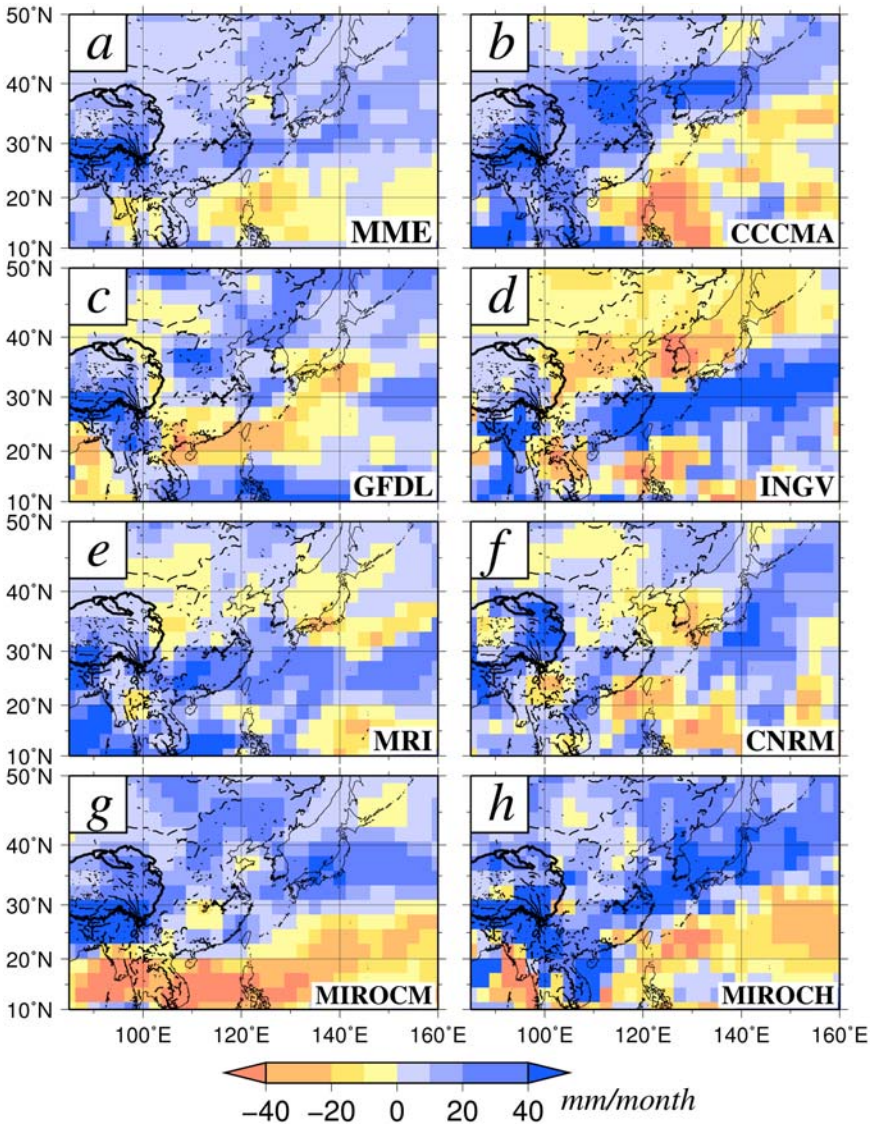

Figure 4. Difference in the 30-year mean precipitation in June between the 20C3M and SRES A1B scenario. Blue represents the increase of precipitation under the SRES-A1B scenario.

in situ stations provided by the Meteorological Administration of China and Automated Meteorological Data Acquisition System (AMeDAS) provided by JMA in Japan. Heavy precipitation exceeding 420 mm/month is observed over the south of the Yangtze River basin (28°N, 118°E)

Table 2. Specifications of the Simulations

Run Name	Initial and Boundary Conditions[a]	Years
CTRL-ERA40	ERA40	1990s
PGW-MIROCM	ERA40+diff_MIROCM	1990s
PGW-MIROCH	ERA40+diff_MIROCH	1990s
PGW-MRI	ERA40+diff_MRI	1990s
PGW-GFDL	ERA40+diff_GFDL21	1990s
PGW-CNRM	ERA40+diff_CNRM	1990s
PGW-CCCMA	ERA40+diff_CCCMA	1990s
PGW-INGV	ERA40+diff_INGV	1990s
PGW-MME	ERA40+diff_MME-CGCM	1990s
PGW-MME-80s	ERA40+diff_MME-CGCM	1980s
CTRL-ERA40-80s	ERA40	1980s
TEMP-RISE	ERA40+ATM3.0K_SST2.2K	1990s

[a]ATM, atmospheric temperature; diff_, difference between the present (1970–1999) and future (2060–2089) climates.

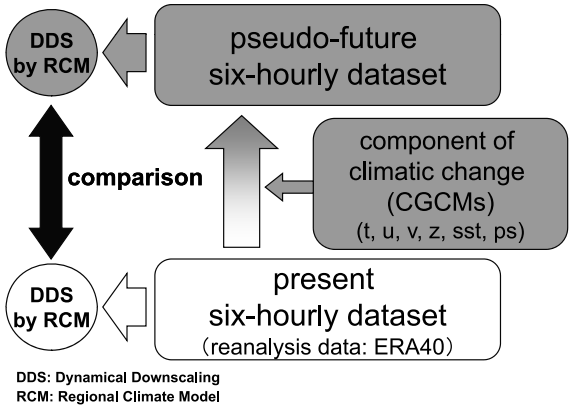

Figure 5. Flowchart of the PGW-DS.

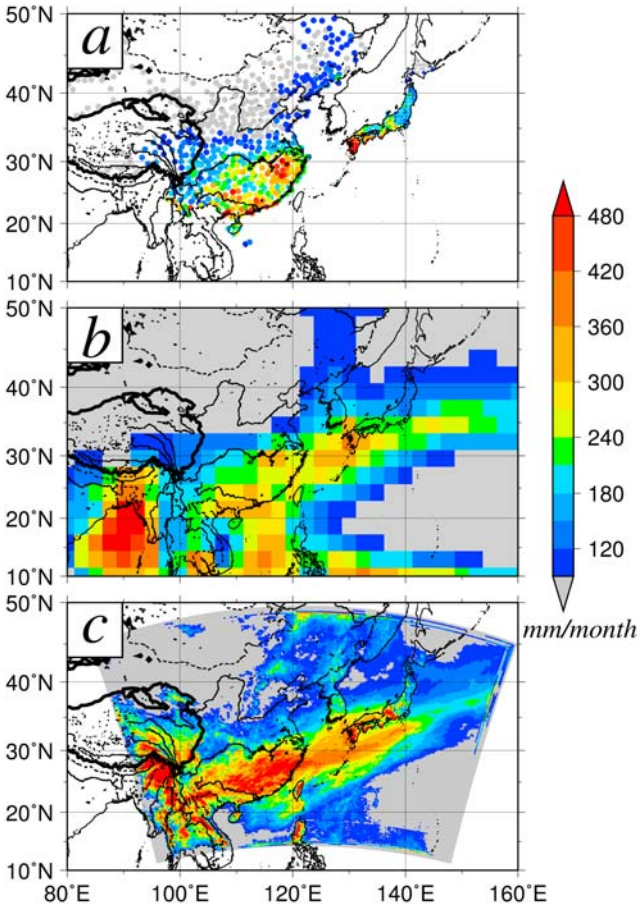

Figure 6. Distributions of 10-year mean precipitation in June during the 1990s (a) observed by in situ stations provided by the Meteorological Administration of China and AMeDAS provided by JMA in Japan, (b) derived from CMAP, and (c) simulated by the CTRL-ERA40 run.

and around the southern coast of China. A large amount of precipitation is also observed over Kyushu in Japan. The amount of precipitation drastically decreases to the north of the Yangtze River. Figure 6b shows the distribution of the 10-year mean precipitation derived from CMAP. The Baiu rainband extends from southern China to Japan.

[24] The CTRL-ERA40 run accurately simulates the Baiu rainband extending from southern China to Japan and the distribution of precipitation in China, e.g., a large amount of precipitation over the south of the Yangtze River basin and the southern coast of China, and a drastic decrease in precipitation to the north of the Yangtze River (Figure 6c). Some previous studies focused on the regional climate modeling without interior or spectral nudging [e.g., *Castro et al.*, 2005]. The climatic fields of wind and geopotential height simulated by the CTRL-ERA40 run without interior or spectral nudging have some small differences from the original ERA40 data. The CTRL-ERA40 run, however, well simulates the location and strength of the Baiu rainband in the 1990s, as shown in Figure 6, which makes it possible to estimate future changes in the Baiu rainband. It should be noted that the amount of precipitation is overestimated, especially around the center of southern China (25°N, 118°E).

4.2. PGW-DS Runs

[25] The Baiu rainbands can be simulated from southern China to Japan in all PGW-DS runs as strongly as in the CTRL-ERA40 run (Figure 7). Most PGW-DS runs shows that the amount of precipitation increases over the southern parts of the Baiu rainband but decreases over the northern parts of the Baiu rainband (Figures 7 and 8). This feature is strongly simulated by the PGW-INGV run (Figure 8d) but is not clear in the PGW-MIROCH and PGW-MIROCM runs in which precipitation increases over the Baiu rainband (Figures 8g and 8h).

[26] Figure 9 shows the interannual variability of the regional mean precipitation in June over region B shown in Figure 1. Region B is wide enough for almost of the precipitation around the Baiu rainband to be detected. The amounts of precipitation simulated by the PGW-MME and PGW-DS runs are 10–50 mm/month larger than that simulated by the CTRL-ERA40 run. The PGW-MME and individual PGW-DS runs show similar interannual variability to the CTRL-ERA40 run. The PGW-MIROCH, however, simulated more precipitation than the other PGW-DS runs in 1993 and 1997. The PGW-INGV also simulated more precipitation in 1991 and 1993. It is noteworthy that the average of the seven PGW-DS runs (hereafter, MME-PGW-DS) shows quite similar interannual variability to the PGW-MME run.

[27] Figure 10 shows the latitudinal distributions of the zonal mean precipitation, which is averaged every 2.5 degrees over region B, in June during the 1990s and pseudo warmed 1990s. The maximum precipitation of about 280 mm/month, which signals the peak of the Baiu rainband, appears at around 27.5°N–30°N in the CTRL-ERA40 run. However, the maxima appear at around 25°N–27.5°N in the PGW-MME run and most PGW-DS runs. The precipitation increases over the southern part of the control Baiu rainband simulated by the CTRL-ERA40 run (20°N–27.5°N). Only the PGW-MIROCM and PGW-MIROCH runs show an increase in precipitation over the control Baiu rainband. The MME-PGW-DS shows quite a similar change to the PGW-MME run as well as the interannual variability of the regional mean precipitation (Figure 9).

4.3. Comparison Between PGW-DS Runs and CGCMs

[28] We compare the intermodel variability in the change of precipitation simulated by the PGW-DS runs (Figures 7 and 8) and projections of the CGCMs (Figures 3 and 4) with the aid of the Taylor diagram [*Taylor*, 2001]. The observational data are applied to the reference data in the original Taylor diagram (see section 2 and Figure 2), while the MME-CGCM and the MME-PGW-DS are applied to the reference data here. We call this Taylor diagram the "MME Taylor diagram." It should be noted that the MME Taylor diagram cannot be used to evaluate the performances of the models in the future climate. The skill score, which shows the skill of CGCM in the original Taylor diagram, refers to the similarity among the models and the MME mean in the MME Taylor diagram. The skill score is called a "similarity score" in the MME Taylor diagram. The models with high (low) similarity scores show similar features to (different features from) the MME mean. When all models have high (low) similarity scores, the intermodel variability is small (large). When the variance of the MME mean is much

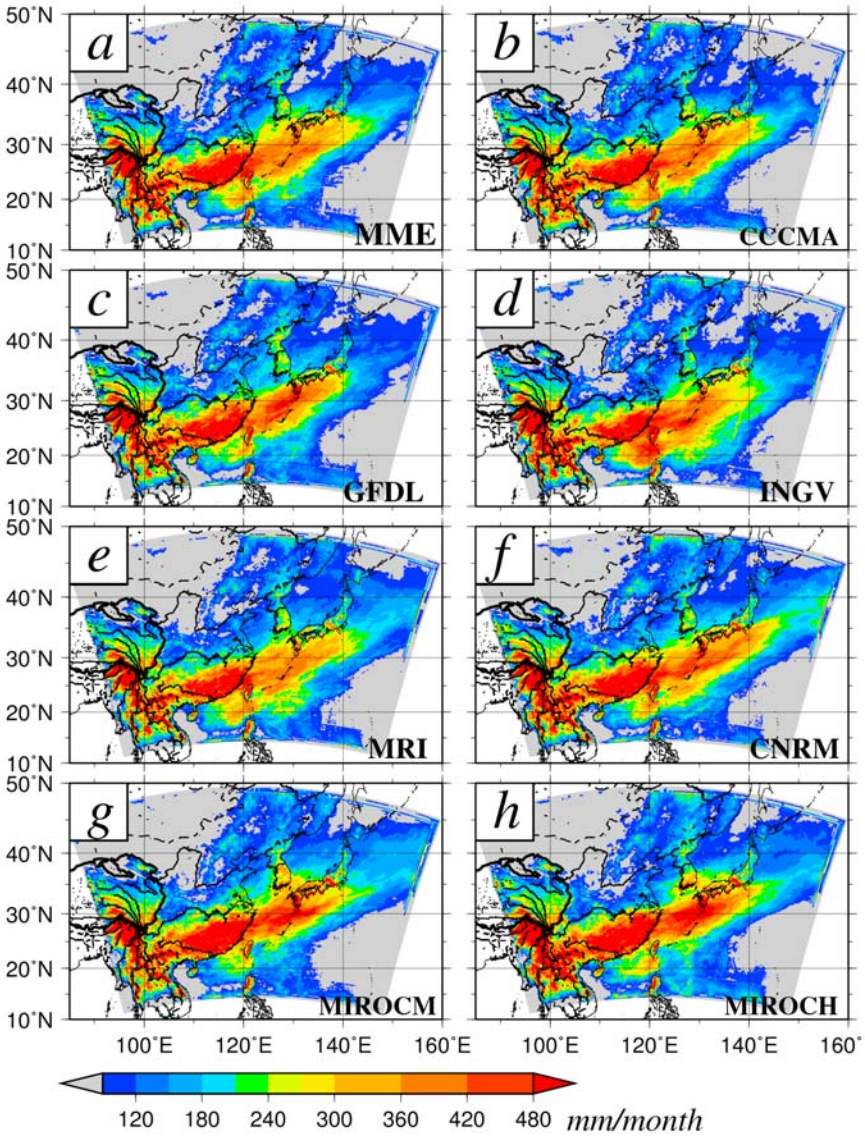

Figure 7. Distributions of June precipitation simulated by the seven PGW-DS runs and the PGW-MME run.

smaller than those of the individual models, all models have different features.

[29] Figure 11 shows the MME Taylor diagrams for the spatial distribution of precipitation in the future climate (Figures 11a and 11c) and the difference in precipitation among the present and future climates (Figures 11b and 11d). Figures 11a and 11b show the projections of the CGCMs and Figures 11c and 11d show the results of the PGW-DS runs. Figures 11a, 11b, 11c, and 11d correspond to Figures 3, 4, 7, and 8, respectively. The similarity scores for the precipitation in the CGCMs are lower than 0.7 (Figure 11a). The CCCMA, MIROCH, and MRI have smaller similarity scores than the other models, which indicates that their projections are far from the MME-CGCM. The location of the rainband in the CCCMA is quite different from that in the MME-CGCM (Figures 3a and 3b), which results in the lowest correlation coefficient and the smallest similarity scores. The variances in the MIROCH and the MRI are higher than those of the others depending on the amount of precipitation around the rainband (Figures 3e and 3h). The similarity scores for the change in precipitation are quite low in all CGCMs (Figure 11b). They are lower than 0.2 except for the MIROCM and the CNRM. The variance of the MME-CGCM is much smaller than those of the seven CGCMs. These results indicate that the seven CGCMs show different changes in the spatial distribution of precipitation, i.e., different changes in the Baiu rainband.

[30] However, all PGW-DS runs show much higher similarity scores than the CGCMs. Their correlation coefficients exceed 0.90 in most PGW-DS runs (Figure 11c). The variances of all PGW-DS runs are comparable to that of the MME-PGW-DS. Even the PGW-MIROCH, PGW-MRI, and PGW-CCCMA show high similarity scores, although their original CGCMs, i.e., MIROCH, MRI, and CCCMA, show quite low similarity scores (Figure 11a). Figure 11c indicates that all PGW-DS runs simulate similar locations and strengths for the Baiu rainband. Moreover, it is note-

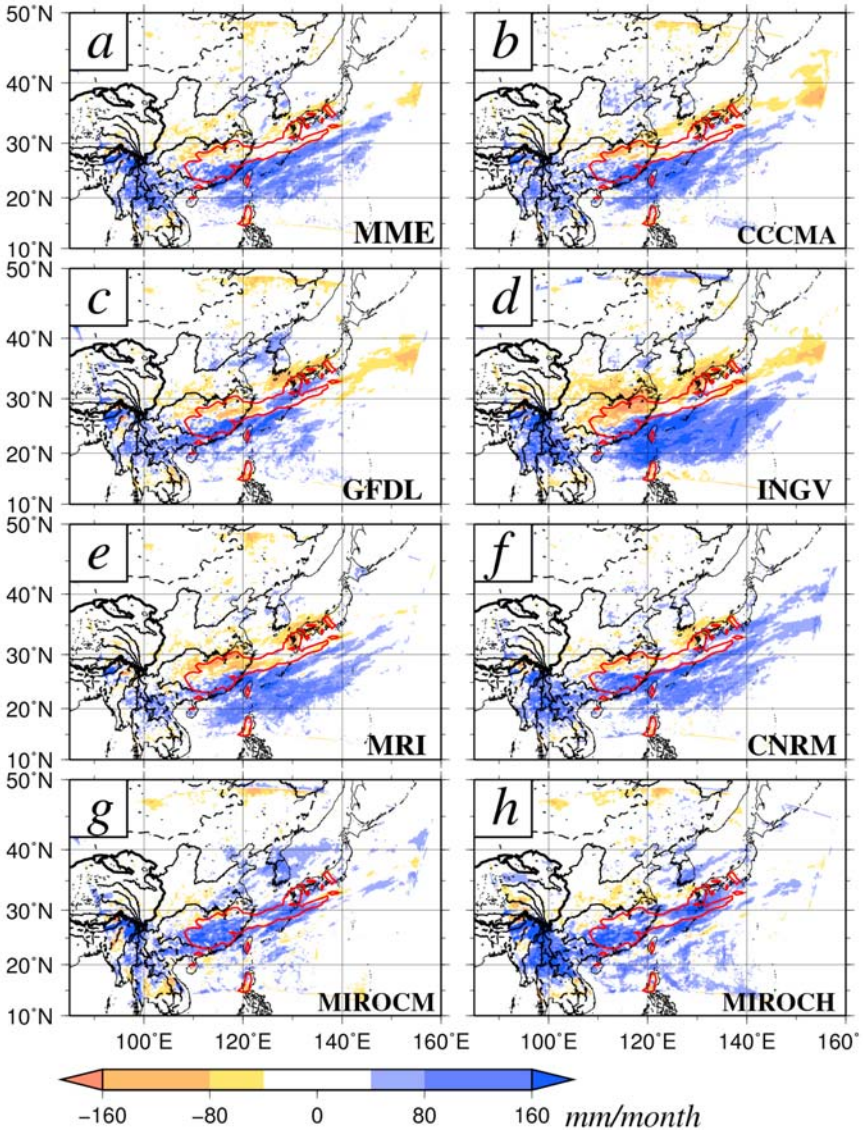

Figure 8. Difference in June precipitation among the CTRL-ERA40 run and each PGW-DS run. Blue indicates that the precipitation in the PGW-DS runs is larger than that in the CTRL-ERA40 run. The areas enclosed by red lines represent the heavy rainfall areas of over 350 mm/month to the east of 110°E simulated by the CTRL-ERA40 run.

worthy that the PGW-MME run, which is the PGW-DS run using the MME-CGCM, also shows a high similarity score of about 0.96. The similarity scores for the difference in precipitation in the PGW-DS runs are also much higher than those in the CGCMs (Figure 11d). They exceed 0.4, except for PGW-MIROCH and PGW-MIROCM. As in Figure 11c, the PGW-MME run shows a high similarity score of about 0.73. The variances of the PGW-DS runs are comparable to that of the PGW-MME run, except for the PGW-INGV run. The clear contrast of the decrease and increase of precipitation results in the large variance in the PGW-INGV run (Figure 8d). The PGW-MIROCM and PGW-MIROCH runs have low correlation coefficients and low similarity scores because they simulate different changes in the spatial distribution of precipitation compared with the other PGW-DS runs and the PGW-MME run (Figure 8). Figure 11 suggests that the PGW-DS runs decrease the intermodel variability in the Baiu rainband relative to the original CGCMs.

5. Discussion

[31] A significant assumption of the PGW-DS is the neglect of changes in variability, such as interannual variability, in the future climate. The future changes in the amplitudes of the interannual variability obtained by selected CGCMs and their uncertainty were investigated in regard to the geopotential height at three pressure levels (850 hPa, 500 hPa, and 200 hPa) over region B shown in Figure 1. We estimated the difference in the standard deviation of interannual variability (hereafter, DSDIV) between the present climate (1970–1999) and the future climate (2060–2089) simulated by each CGCM as well as the DSDIV between ERA40 data and each CGCM in the present climate. The

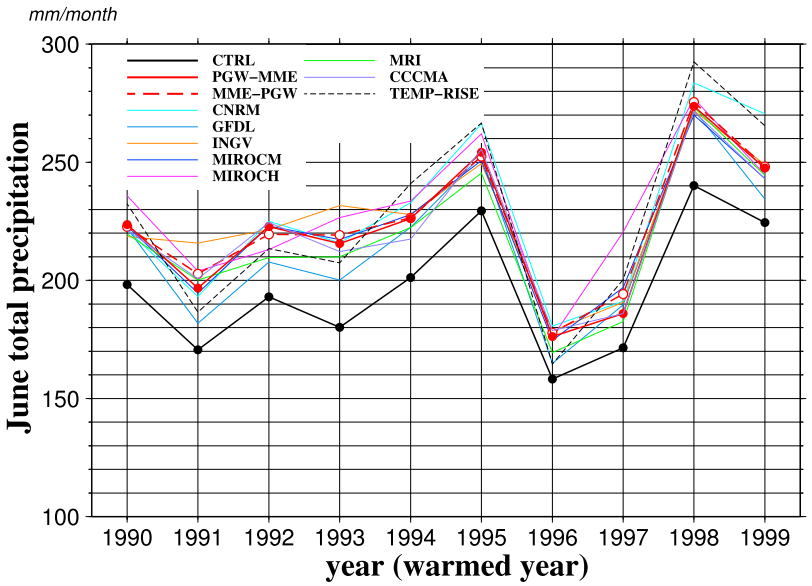

Figure 9. Time series of the regional mean precipitation in June over region B shown in Figure 1. A solid black line represents the CTRL-ERA40 run. The solid and dashed red lines represent the PGW-MME run and the average of all PGW-DS runs, respectively. The other colored lines represent the individual PGW-DS runs. The dashed black line represents the TEMP-RISE run.

DSDIVs between the present and the future climates were comparable to those between ERA40 data and the individual CGCMs in the present climate at all of three pressure levels. These facts indicate that the uncertainty of CGCMs is too large to discuss the change in the amplitudes of the interannual variability. In addition, the mean of the DSDIVs between the present and future climates among the CGCMs was much smaller than the standard deviation of the DSDIVs among the CGCMs. These results suggest that the signal of the change in the amplitudes of the interannual variability is insignificant in the CGCMs.

[32] The PGW-DS based on other decades, such as the 1970s and the 1980s, may simulate the different changes in the Baiu rainband from those simulated by the PGW-DS based on the 1990s. We conducted the additional control run (hereafter, CTRL-ERA40-80s run) and the PGW-MME run (hereafter, PGW-MME-80s run) in the 1980s. Here, the PGW-MME-80s run is expected to represent the average of all PGW-DS runs using individual CGCMs in the 1980s (see Figures 9 and 10).

[33] The CTRL-ERA40-80s simulates the Baiu rainband extending from southern China to Japan (Figure 12a). In comparison with the 1990s, the location of the Baiu rainband is similar to that in the 1990s, while the amount of precipitation is smaller than that in the 1990s, which is also shown in observational data (figure not shown). Figure 12b

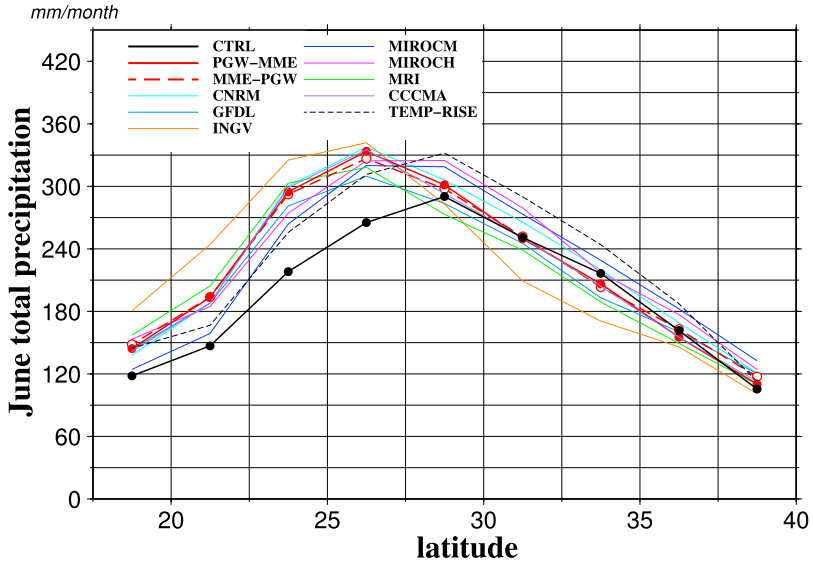

Figure 10. Latitudinal distribution of the 10-year mean precipitation in June averaged over 90°E–150°E and every 2.5 degrees. All lines are the same as those in Figure 9.

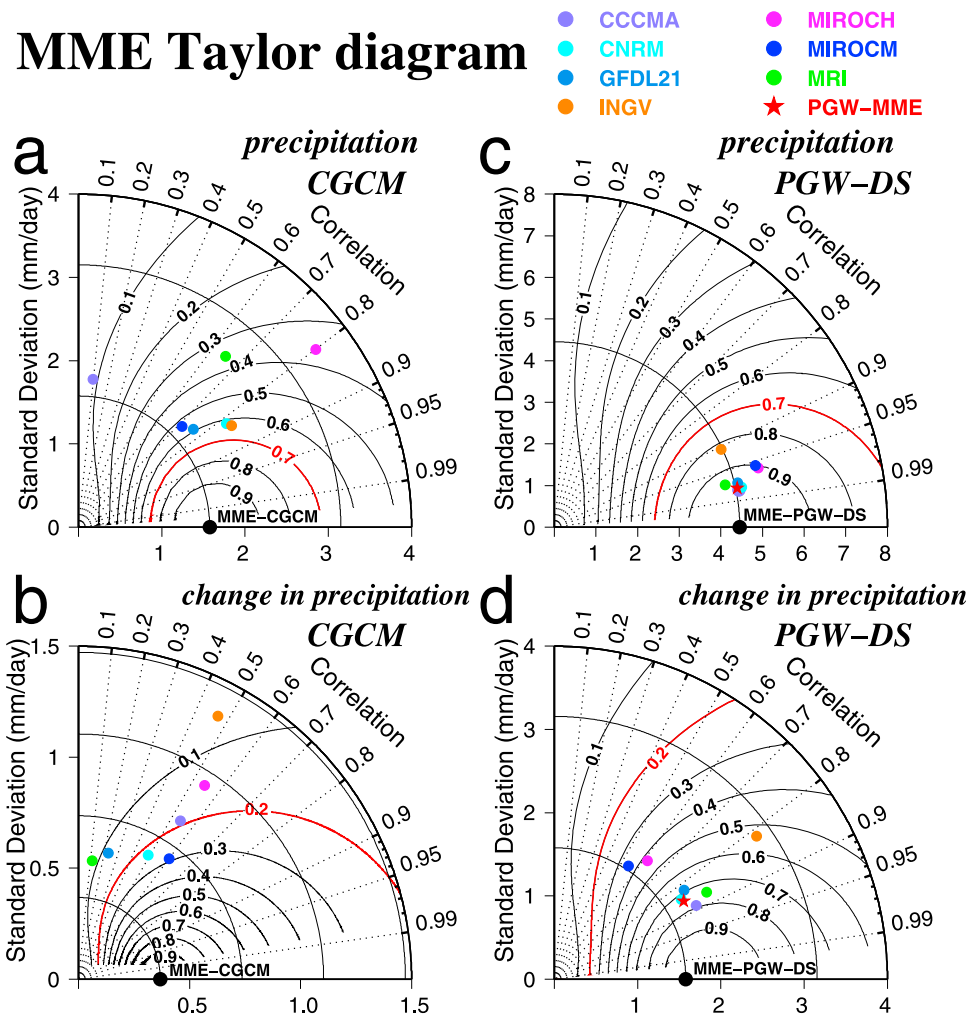

Figure 11. MME Taylor diagrams for the 10-year mean precipitation in June projected by (a) the CGCMs and (c) the PGW-DS runs and changes in precipitation projected by (b) the CGCMs and (d) the PGW-DS runs.

shows the difference in precipitation in the CTRL-ERA40-80s and PGW-MME-80s runs. Precipitation increases over the southern part of the control Baiu rainband, which suggests the southward shift of the Baiu rainband. It is noteworthy that the change in the Baiu rainband simulated by the PGW-MME-80s run is quite similar to the PGW-MME run based on the 1990s (Figure 8a). In consideration with the mechanism to form the Baiu rainband, it is unlikely that the Baiu rainband locates at a quite different place in the other present decades. The results suggest that the PGW-DS is expected to obtain similar results regardless of the selected decade.

[34] These facts also suggest that the selection of reanalysis data, such as ERA40 data, the National Centers for Environmental Prediction/National Center for Atmospheric Research (NCEP/NCAR) reanalysis data, and Japanese 25-year Reanalysis (JRA25) data, would not affect the results of the PGW-DS run. The differences in the reanalysis data are much smaller than those between decades, e.g., the 1980s and the 1990s.

[35] An increase in temperature owing to global warming would contribute to the change in the Baiu rainband because of the increase of the saturation vapor pressure. The PGW-DS assumes that the relative humidity of the future climate would be equal to that of the present climate, which results in an increase in the absolute value of water vapor in the warm future climate following the Clausius-Clapeyron relationships. The impact of a temperature rise on the Baiu rainband is estimated by the TEMP-RISE run assuming only an atmospheric and sea surface temperature rise (see section 3).

[36] The dashed black lines in Figures 9 and 10 show the results of the TEMP-RISE run. The regional mean precipitation increases, as in the PGW-DS runs (Figure 9), while the amount of precipitation increases at almost the same rate at all latitudes (Figure 10). The southward shift of the Baiu rainband, which is shown in most PGW-DS runs, is not simulated by the TEMP-RISE run. The TEMP-RISE run suggests that the temperature rise would contribute to the increase of precipitation around the Baiu rainband, while the other factors of the PGW-DS runs would influence the shift of the Baiu rainband. It must be noted that we only indicated the direct effect of the temperature rise in the regional scale shown in Figure 1 without considering the indirect effect accompanied with the SST rise, such as the global-scale atmospheric response to the El Nino con-

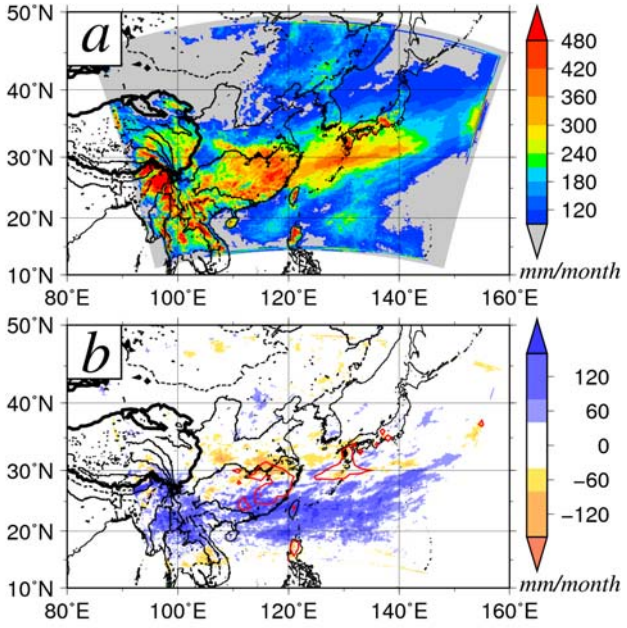

Figure 12. Distribution of (a) June precipitation simulated by the CTRL-ERA40-80s run and (b) difference in June precipitation between the CTRL-ERA40-80s run and the PGW-MME-80s run. The areas enclosed by red lines represent the heavy rainfall areas of over 350 mm/month to the east of 110°E simulated by the CTRL-ERA40-80s run.

ditions of the ocean pointed out in previous studies [e.g., *Kitoh et al.*, 2005].

[37] The change in the location of the Baiu rainband is thought to be affected by the change in the large-scale circulation projected by the CGCMs throughout the lateral boundary of the RCM. *Ninomiya* [2000] suggested that the differential advection of the equivalent potential temperature, which consists of a poleward moisture flux by the low-level jet and cold air advection by the upper-level jet, is a primary factor in the formation of the active Baiu rainband. *Yoshikane et al.* [2001] reported that the Baiu rainband is quite sensitive to the positions of the upper-level jet and the low-level jet. It is suggested that the future change in summer precipitation in East Asia will be attributable to the change in the lower moisture flux and its convergence associated with the subtropical high [*Kurihara et al.*, 2005].

[38] Figure 13 shows the difference of the moisture flux at 850 hPa between the CTRL-ERA40 run and the PGW-MME run. Contour lines represent the zero vorticity at 200 hPa, which mean the axes of the upper-level jet. The poleward moisture flux increases around the southwestern boundary of the model domain (15°N, 115°E). The eastward to northeastward moisture flux also increases over the northeastern Pacific Ocean (115°E–145°E, 20°N–30°N). The increase of the lower-level moisture flux enhances the convective instability, resulting in more precipitation around the Baiu rainband in the PGW-MME run than that in the CTRL-ERA40 run. However, the zero vorticity contour line shifts southward (110–140°E), which means that the meandering of the upper-level jet is more remarkable in the PGW-MME run than that in the CTRL-ERA40 run. The larger amplitude of the meandering brings cold air more southward in the upper level. It can be summarized that the enhancement and the southward shift of the Baiu rainband are the results of the change in the differential advection of equivalent potential temperature caused by two factors: (1) the increase of the northeastward moisture flux over the northwestern Pacific Ocean at the lower level, and (2) the increase of the southward cold air advection in the upper level. However, detailed mechanisms in the shift of the Baiu rainband are still unknown. Further studies are needed to identify them.

[39] One major problem is the projection of typhoons in the future climate that would sometimes strongly affect the

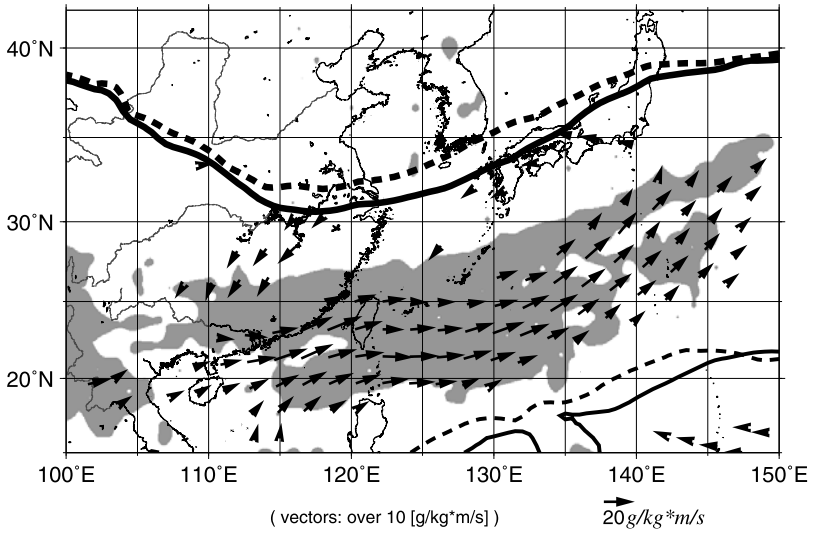

Figure 13. Difference of the moisture flux at 850 hPa between the CTRL-ERA40 run and the PGW-MME run (vector) and the zero vorticity contours at 200 hPa simulated by the CTRL-ERA40 (bold dashed line) and PGW-MME runs (bold solid line) in June. The gray shading indicates that the amount of precipitation in the PGW-MME run is 40 mm larger than that in the CTRL-ERA40 run.

amount of precipitation during the Baiu season. The PGW-DS may not estimate the impact of a typhoon accurately because of the assumption of PGW-DS on the boundary conditions. To reduce the uncertain impacts of a typhoon, this study focuses on only June, when there are fewer typhoons than in the other months. Since several typhoons annually approach Japan and China from July to September, extreme care must be exercised regarding typhoons when the PGW-DS is conducted in such months. *Knutson et al.* [2008] applied a similar method to the simulation of the Atlantic hurricane frequency using a wide domain for the RCM. The PGW-DS would require a much larger domain than has been assumed here when the PGW-DS estimates the change in the Baiu rainband, including the impact of typhoons.

[40] The PGW-DS assumes unchanged interannual variability and frequencies of disturbances. The change in extreme precipitation events might be affected by them. The usefulness of PGW-DS for extreme events should be examined in future works. We also assume constant relative humidity between the present and future climates. *Rowell and Jones* [2006] suggested that the relative humidity tends to decrease over land in global warming condition owing to the change in large-scale land-sea circulation. The change in the relative humidity in the regional scale would affect the amount and distribution of precipitation. It is necessary to conduct further PGW-DSs to investigate the impact of the change in the relative humidity.

[41] The PGW-DS has some limitations in the assessment of future projections. However, the PGW-DS can reduce the intermodel variability of changes in the Baiu rainband and contribute to the reduction of uncertainty in the climate changes projected by multiple CGCMs.

6. Conclusion

[42] For the estimation of the change in the Baiu rainband owing to global warming, multiple PGW-DS runs were conducted using selected CMIP3 multimodel data set giving better performance around East Asia in June. Most PGW-DS runs and the PGW-MME run, which is the PGW-DS run using the multiple CGCM ensemble mean, simulated an increase in precipitation over the Baiu rainband and the southward shift of the Baiu rainband. The PGW-MME run has good similarity to the average of all PGW-DS runs, e.g., the change in the regional mean precipitation and the shift of the Baiu rainband. These facts suggest that the average of the multiple PGW-DS runs can be replaced by a single PGW-DS using the multiple CGCM ensemble mean, which significantly reduces the computational expense. The PGW-MME run based on the 1980s simulated the change in the Baiu rainband with considerable similarity to the PGW-MME run based on the 1990s, suggesting that the PGW-DS is expected to obtain similar results regardless of the selection of control decade. The comparison of the PGW-DS runs and the CGCM projections suggests that the PGW-DS runs reduce the intermodel variability in the Baiu rainband caused by CGCMs themselves. Although the PGW-DS assumes an unchanged variability in the future climate, the PGW-DS can be used as a new method to assess the regional climate changes owing to global warming.

[43] **Acknowledgments.** This work was supported by the Global Environment Research Fund (B-061) of the Ministry of the Environment and Ministry of Education, Culture, Sports, Science, and Technology of Japan. H. Ueda, T. Inoue, and F. Kimura were supported by the Global Environment Research Fund (S-5-2 and S-5-3) of the Ministry of the Environment of Japan in the course of this work. We acknowledge the modeling groups, the Program for Climate Model Diagnosis and Intercomparison, and the World Climate Research Program's (WCRP) Working Group on Coupled Modeling for their roles in making the WCRP Coupled Model Intercomparison Project Phase 3 multimodel data set available. Support of this data set was provided by the Office of Science, U.S. Department of Energy. This work was jointly supported by the China National Key Planning Development for Basic Research (grant 2006CB400500). We appreciate I. Takayabu in the Meteorological Research Institute for his helpful suggestions. We also thank three anonymous reviewers for their precise and useful comments.

References

Castro, C. L., R. A. Pielke Sr., and G. Leoncini (2005), Dynamical downscaling: Assessment of value retained and added using the Regional Atmospheric Modeling System (RAMS), *J. Geophys. Res.*, *110*, D05108, doi:10.1029/2004JD004721.

Chen, F., and J. Dudhia (2001), Coupling an advanced land-surface/hydrology model with the Penn State/NCAR MM5 modeling system. part I: Model description and implementation, *Mon. Weather Rev.*, *129*, 569–585, doi:10.1175/1520-0493(2001)129<0569:CAALSH>2.0.CO;2.

Dai, A. (2006), Recent climatology, variability and trends in global surface humidity, *J. Clim.*, *19*, 3589–3606, doi:10.1175/JCLI3816.1.

Frei, C., C. Schar, D. Luthi, and H. C. Davies (1998), Heavy precipitation processes in a warmer climate, *Geophys. Res. Lett.*, *25*, 1431–1434, doi:10.1029/98GL51099.

Giorgi, F., and L. O. Mearns (2002), Calculation of average, uncertainty range, and reliability of regional climate changes from AOGCM simulations via the "reliability ensemble averaging" (REA) method, *J. Clim.*, *15*, 1141–1158, doi:10.1175/1520-0442(2002)015<1141:COAURA>2.0.CO;2.

Hara, M., T. Yoshikane, H. Kawase, and F. Kimura (2008), Estimation of the impact of global warming on snow depth in Japan by the pseudo-global-warming method, *Hydrol. Res. Lett.*, *2*, 61–64, doi:10.3178/hrl.2.61.

Hong, S.-Y., and J.-O. J. Lim (2006), The WRF single-moment microphysics scheme (WSM6), *J. Korean Meteorol. Soc.*, *42*, 129–151.

Inoue, T., and H. Ueda (2009), Evaluation for the seasonal evolution of the summer monsoon over the Asian and western North Pacific sector in the WCRP CMIP3 multi-model experiments, *J. Meteorol. Soc. Jpn.*, *87*, 539–560, doi:10.2151/jmsj.87.539.

Intergovernmental Panel on Climate Change (IPCC) (2000), *Special Report on Emissions Scenarios: A Special Report of Working Group III of the Intergovernmental Panel on Climate Change*, edited by N. Nakicenovic and R. Swart, Cambridge Univ. Press, New York.

Intergovernmental Panel on Climate Change (IPCC) (2001), *Climate Change 2001: The Scientific Basis. Contribution of Working Group I to the Third Assessment Report of the Intergovernmental Panel on Climate Change*, edited by J. T. Houghton et al., Cambridge Univ. Press, New York.

Intergovernmental Panel on Climate Change (IPCC) (2007), *Climate Change 2007: The Physical Science Basis. Contribution of Working Group I to the Fourth Assessment Report of the Intergovernmental Panel on Climate Change*, edited by S. Solomon et al., Cambridge Univ. Press, New York.

Janjic, Z. I. (2002), Nonsingular implementation of the Mellor-Yamada level 2.5 scheme in the NCEP meso model, *Off. Note 437*, pp. 1–61, Natl. Cent. for Environ. Prot., Camp Springs, Md.

Kain, J. S., and J. M. Fritsch (1993), Convective parameterization for mesoscale models: The Kain-Fritsch scheme, in *The Representation of Cumulus Convection in Numerical Models*, *Meteorol. Monogr.*, vol. 46, edited by K. Emanuel and D. J. Raymond, pp. 165–170, Am. Meteorol. Soc., Boston, Mass.

Kang, I.-S., et al. (2002), Intercomparison of the climatological variations of Asian summer monsoon precipitation simulated by 10 GCMs, *Clim. Dyn.*, *19*, 383–395, doi:10.1007/s00382-002-0245-9.

Kato, H., K. Nishizawa, H. Hirakuchi, S. Kadokura, N. Oshima, and F. Giorgi (2001), Performance of RegCM2.5/NCAR-CSM nested system for the simulation of climate change in East Asia caused by global warming, *J. Meteorol. Soc. Jpn.*, *79*, 99–121, doi:10.2151/jmsj.79.99.

Kawase, H., T. Yoshikane, M. Hara, B. Ailikun, F. Kimura, and T. Yasunari (2008), Downscaling of the climatic change in the Mei-yu rainband in East Asia by a pseudo climate simulation method, *SOLA*, *4*, 73–76, doi:10.2151/sola.2008-019.

Kawatani, Y., and M. Takahashi (2003), Simulation of the Baiu front in a high resolution AGCM, *J. Meteorol. Soc. Jpn.*, *81*, 113–129, doi:10.2151/jmsj.81.113.

Kimoto, M. (2005), Simulated change of the East Asian circulation under global warming scenario, *Geophys. Res. Lett.*, *32*, L16701, doi:10.1029/2005GL023383.

Kimoto, M., N. Yasutomi, C. Yokoyama, and S. Emori (2005), Projected changes in precipitation characteristics around Japan under the global warming, *SOLA*, *1*, 85–88, doi:10.2151/sola.2005-023.

Kimura, F., and A. Kitoh (2007), Downscaling by pseudo global warming method, *Final Rep.*, pp. 43–46, ICCAP, Res. Inst. for Humanity and Nat., Kyoto, Japan.

Kitoh, A., and T. Uchiyama (2006), Changes in onset and withdrawal of the East Asian summer rainy season by multi-model global warming experiments, *J. Meteorol. Soc. Jpn.*, *84*, 247–258, doi:10.2151/jmsj.84.247.

Kitoh, A., M. Hosaka, Y. Adachi, and K. Kamiguchi (2005), Future projections of precipitation characteristics in East Asia simulated by the MRI CGCM2, *Adv. Atmos. Sci.*, *22*, 467–478, doi:10.1007/BF02918481.

Knutson, T. R., J. J. Sirutis, S. T. Garner, G. A. Vecchi, and I. M. Held (2008), Simulated reduction in Atlantic hurricane frequency under twenty-first-century warming conditions, *Nat. Geosci.*, *1*, 359–364, doi:10.1038/ngeo202.

Kurashima, A., and Y. Hiranuma (1971), *Synoptic and Climatological Study on the Upper Moist Tongue Extending From Southeast Asia to the East Asia Water Balance of Monsoon Asia*, edited by M. M. Yoshino, pp. 153–169, Univ. of Tokyo Press, Tokyo.

Kurihara, K., K. Ishihara, H. Sasaki, Y. Fukuyama, H. Saitou, I. Takayabu, K. Murazaki, Y. Sato, S. Yukimoto, and A. Noda (2005), Projection of climate change over Japan due to global warming by a high-resolution regional climate model in MRI, *SOLA*, *1*, 97–100, doi:10.2151/sola.2005-026.

Kusunoki, S., J. Yoshimura, H. Yoshimura, A. Noda, K. Oouchi, and R. Mizuta (2006), Change of Baiu rain band in global warming projection by an atmospheric general circulation model with a 20-km grid size, *J. Meteorol. Soc. Jpn.*, *84*, 581–611, doi:10.2151/jmsj.84.581.

Meehl, G. A., C. Covey, T. Delworth, M. Latif, B. McAvaney, J. F. B. Mitchell, R. J. Stouffer, and K. E. Taylor (2007), The WCRP CMIP3 multimodel dataset: A new era in climate change research, *Bull. Am. Meteorol. Soc.*, *88*, 1383–1394, doi:10.1175/BAMS-88-9-1383.

Min, S.-K., E.-H. Park, and W.-T. Kwon (2004), Future projections of East Asian climate change from multi-AOGCM ensembles of IPCC SRES scenario simulations, *J. Meteorol. Soc. Jpn.*, *82*, 1187–1211, doi:10.2151/jmsj.2004.1187.

Mizuta, R., K. Oouchi, H. Yoshimura, A. Noda, K. Katayama, S. Yukimoto, M. Hosaka, S. Kusunoki, H. Kawai, and M. Nakagawa (2006), 20-km-mesh global climate simulations using JMA-GSM model-mean climate states, *J. Meteorol. Soc. Jpn.*, *84*, 165–185, doi:10.2151/jmsj.84.165.

Ninomiya, K. (2000), Large- and meso-α-scale characteristics of Meiyu/Baiu front associated with intense rainfalls in 1–10 July 1991, *J. Meteorol. Soc. Jpn.*, *78*, 141–157.

Ninomiya, K., T. Nishimura, W. Ofuchi, T. Suzuki, and S. Matsumura (2002), Features of the Baiu front simulated in an AGCM (T42L52), *J. Meteorol. Soc. Jpn.*, *80*, 697–716, doi:10.2151/jmsj.80.697.

Rowell, D. P., and R. G. Jones (2006), Causes and uncertainty of future summer drying over Europe, *Clim. Dyn.*, *27*, 281–299, doi:10.1007/s00382-006-0125-9.

Sato, T., F. Kimura, and A. Kitoh (2007), Projection of global warming onto regional precipitation over Mongolia using a regional climate model, *J. Hydrol.*, *333*, 144–154, doi:10.1016/j.jhydrol.2006.07.023.

Skamarock, W. C., J. Dudhia, D. O. Gill, D. M. Barker, W. Wang, and J. G. Powers (2005), A description of the Advanced Research WRF version 2, *NCAR Tech. Note TN-468*, 100 pp., Natl. Center for Atmos. Res., Boulder, Colo.

Soden, B. J., D. L. Jackson, V. Ramaswamy, D. Schwarzkopf, and X. Huang (2005), The radiative signature of upper tropospheric moistening, *Science*, *310*, 841–844, doi:10.1126/science.1115602.

Taylor, K. E. (2001), Summarizing multiple aspects of model performance in a single diagram, *J. Geophys. Res.*, *106*, 7183–7192, doi:10.1029/2000JD900719.

Trenberth, K. E. (2005), The impact of climate change and variability on heavy precipitation, floods, and droughts, in *Encyclopedia of Hydrological Sciences*, edited by M. G. Anderson, John Wiley, Hoboken, N. J., doi:10.1002/0470848944.hsa211.

Ueda, H., A. Iwai, K. Kuwako, and M. E. Hori (2006), Impact of anthropogenic forcing on the Asian summer monsoon as simulated by eight GCMs, *Geophys. Res. Lett.*, *33*, L06703, doi:10.1029/2005GL025336.

Uppala, S. M., et al. (2005), The ERA-40 re-analysis, *Q. J. R. Meteorol. Soc.*, *131*, 2961–3012, doi:10.1256/qj.04.176.

Wang, Y. Q., L. R. Leung, J. L. McGregor, D.-K. Lee, W.-C. Wang, Y. H. Ding, and F. Kimura (2004), Regional climate modeling: Progress, challenges, and prospects, *J. Meteorol. Soc. Jpn.*, *82*, 1599–1628, doi:10.2151/jmsj.82.1599.

Xie, P., and P. A. Arkin (1997), Global precipitation: A 17-year monthly analysis based on gauge observation, satellite estimates, and numerical model outputs, *Bull. Am. Meteorol. Soc.*, *78*, 2539–2558, doi:10.1175/1520-0477(1997)078<2539:GPAYMA>2.0.CO;2.

Yasunaga, K., et al. (2006), Changes in the Baiu frontal activity in the future climate simulated by super-high-resolution global and cloud-resolving regional climate models, *J. Meteorol. Soc. Jpn.*, *84*, 199–220, doi:10.2151/jmsj.84.199.

Yoshikane, T., F. Kimura, and S. Emori (2001), Numerical study on the Baiu front genesis by heating contrast between land and ocean, *J. Meteorol. Soc. Jpn.*, *79*, 671–686, doi:10.2151/jmsj.79.671.

Yoshizaki, M., C. Muroi, S. Kanada, Y. Wakazuki, K. Yasunaga, A. Hashimoto, T. Kato, K. Kurihara, A. Noda, and S. Kusunoki (2005), Changes of Baiu (Mei-yu) frontal activity in the global warming climate simulated by a cloud-resolving non-hydrostatic regional model, *SOLA*, *1*, 25–28, doi:10.2151/sola.2005-008.

B. Ailikun, Institute of Atmospheric Physics, Chinese Academy of Science, Qijiahuozi Huayanli 40, Chaoyang District, PO Box 9804, Beijing 100029, China.

M. Hara, F. Kimura, and T. Yoshikane, Research Institute for Global Change, Japan Agency for Marine-Earth Science and Technology, 3173-25 Showamachi, Kanazawa-ku, Yokohama, Kanagawa 236-0001, Japan.

T. Inoue and H. Ueda, Graduate School of Life and Environmental Sciences, University of Tsukuba, Tennoudai 1-1-1, Tsukuba, Ibaraki 305-8577, Japan.

H. Kawase, Atmospheric Physics Section, Atmospheric Environment Division, National Institute for Environmental Studies, 16-2 Onogawa, Tsukuba, Ibaraki 305-8506, Japan. (kawase.hiroake@nies.go.jp)

T. Yasunari, Hydrospheric Atmospheric Research Center, Nagoya University, Furo-cho, Chikusa-ku, Nagoya 464-8601, Japan.